Structural and Multidisciplinary Optimization (2019) 59:1655–1671
https://doi.org/10.1007/s00158-018-2151-8

RESEARCH PAPER

A new method for reliability analysis and reliability-based design optimization

Alfredo Canelas[1] · Miguel Carrasco[2] · Julio López[3]

Received: 25 July 2018 / Revised: 1 October 2018 / Accepted: 11 November 2018 / Published online: 4 January 2019

Abstract

We present a novel method for reliability-based design optimization, which is based on the approximation of the safe region in the random space by a polytope-like region. This polytope is in its turn transformed into quite a simple region by using generalized spherical coordinates. The failure probability can then be easily estimated by considering simple quadrature rules. One of the advantages of the proposed approach is that by increasing the number of vertices, we can improve arbitrarily the accuracy of the failure probability estimation. The sensitivity analysis of the failure probability is also provided. We show that the proposed approach leads to an optimization problem, where the set of optimization variables includes all the original design variables and all the parameters that control the shape of the polytope. In addition, this problem can be solved by a single iteration scheme of optimization. We illustrate the performance of the new approach by solving several examples of truss topology optimization.

Keywords Reliability-based design · Truss topology optimization · Stochastic structural model

1 Introduction

According to Choi et al. (2007), the study of structural reliability is concerned with the calculation and prediction of the probability of limit-state violations, at any stage during a structure's life. The *reliability analysis* is the application of known mathematical and engineering procedures with the purpose to model uncertainties, and obtain quantitative information about their effect on the structural behavior. In particular, the reliability analysis provides the estimation of the probability of limit-state violation, also called *failure probability*. Reliability-based design optimization (RBDO) is a subtopic of design optimization, where we look for an optimal design that must satisfy certain specified constraint related to the failure probability. There is a vast literature about RBDO, and we refer the reader to references (Choi et al. 2007; Ditlevsen and Madsen 1996; Schuëller and Jensen 2008). A generic formulation of a RBDO problem is as follows:

$$\begin{aligned} &\min_{\mathbf{x}} f(\mathbf{x}), \\ &\text{s.t. } \mathbb{P}\{\Omega(\mathbf{x})\} \geq 1 - P_f\,, \\ &\mathbf{h}(\mathbf{x}) \leq 0\,. \end{aligned} \qquad (P)$$

In the previous problem, $\mathbf{x} \in \mathbb{R}^n$ is the vector of design variables, f is the objective function, $\mathbb{P}\{\cdot\}$ is the probability function, $\Omega(\mathbf{x})$ is the *safe region* in the random space, P_f is a given upper bound on the failure probability, and $\mathbf{h}$ is the vector function of deterministic constraints on the design variable. The probability $\mathbb{P}\{\Omega(\mathbf{x})\}$ is called *reliability* of the design $\mathbf{x}$, while $1 - \mathbb{P}\{\Omega(\mathbf{x})\}$ is the failure probability. The safe region is given by

$$\Omega(\mathbf{x}) = \{\boldsymbol{\xi} \in \mathbb{R}^m \ : \ \mathbf{g}(\mathbf{x}, \boldsymbol{\xi}) \leq 0\},$$

where $\boldsymbol{\xi}$ is the vector of random variables and $\mathbf{g}(\mathbf{x}, \boldsymbol{\xi})$ is the vector of limit state functions, i.e., for the design $\mathbf{x}$, $\boldsymbol{\xi}$ is considered a failure realization if any component $g_i(\mathbf{x}, \boldsymbol{\xi}) >$

Responsible Editor: Byeng D Youn

✉ Alfredo Canelas
acanelas@fing.edu.uy

[1] Facultad de Ingeniería, Instituto de Estructuras y Transporte, Universidad de la República, Julio Herrera y Reissig 565, Montevideo, Uruguay

[2] Facultad de Ingeniería y Ciencias Aplicadas, Universidad de los Andes, Mons. Álvaro del Portillo, Las Condes, 12455 Santiago, Chile

[3] Facultad de Ingeniería y Ciencias, Universidad Diego Portales, Avda. Ejército 441, Santiago, Chile

0. The probability density function $f_{\boldsymbol{\xi}}$ associated to the random variable $\boldsymbol{\xi}$ provides a mathematical expression for the reliability:

$$\mathbb{P}\{\Omega(\mathbf{x})\} = \int_{\Omega(\mathbf{x})} f_{\boldsymbol{\xi}}\, d\boldsymbol{\xi}\,. \tag{1}$$

It is usually assumed that $\boldsymbol{\xi}$ corresponds to a multivariate normal distribution. This assumption does not imply a severe loss of generality, since other types of distribution can be related to the normal distribution through a nonlinear change of variables.

Problem (P) is usually rather hard to solve, since any evaluation of the probability constraint required in the iterative optimization process implies an entire reliability analysis of the current design. Methods for this include those called sampling methods, such as Monte Carlo Simulation, Stochastic Finite Element Method, others based on stochastic expansions, etc. There are also methods that directly try to compute (1) in an approximate manner, e.g., the *first order reliability method* (FORM), and the *second order reliability method* (SORM), which are two of the most popular ones for reliability assessment in RBDO. In the case of a single limit state function, the main idea behind FORM is to approximate the safe region $\Omega(\mathbf{x})$ by a half space, for which the probability can be easily calculated in the case of a multivariate normal distribution. The half space considered is defined by the tangent plane to the *limit state surface* $\partial\Omega(\mathbf{x})$ at the point that is closest to the origin, which is called *most likely failure point* and also *most probable point* (MPP). In the case of SORM, the safe region is approximated in a similar manner by considering a second order approximation of the limit state surface. SORM is then more expensive than FORM, since in addition to the MPP, it requires information about the curvatures of the limit state surface at the MPP. When several limit state functions have to be considered, multi-point versions of FORM and SORM consist to find the MPP and the corresponding approximation of each limit state surface. Then, for the reliability estimation, FORM and SORM rely on accurate approximate expressions that provide the probability of intersections of multiple half spaces. These expressions are easy to compute, so that the most expensive task in FORM and SORM procedures is the determination of all the MPPs.

According to Rackwitz (2001), FORM and SORM are well established methodologies that provide the failure probability with an acceptable error in view of the large uncertainty in selecting the appropriate stochastic model and its parameters. However, it is known that optimization strategies based in FORM or SORM can still fail to find the optimal design. On the one hand, the optimization strategy used to find the MPP can fail, e.g., in the case of convergence to local minima. On the other hand, even if the MPP is correctly located, the estimations of the failure probability can be inaccurate, which occurs when the approximate regions badly represent the real ones. It is know that *important sampling* can be used to improve the accuracy of results (Rackwitz 2001). However, in the case of symmetric safe regions, FORM underestimates the failure probability, since it ignores completely the half space corresponding to the point that is symmetric to the MPP found (Liu et al. 2016a). In some cases, the sensitivities of the failure probability are badly estimated. For instance, Liu et al. (2016a) mention the case of a perturbation of the design variables that keeps the MPP and the tangent plane unchanged. In this case, FORM would erroneously report zero sensitivities. To improve the accuracy of the estimations, Liu et al. (2016b) introduced segmental multi-point linearization method (SML), that instead of considering a single plane as is done in FORM (or a single smooth surface in the case of SORM) fits the limit state surface segmentally with multiple linear pieces. A rather simple version of the SML, that consists of fitting the limit state surface with an orthogonal box, was used by Liu et al. (2016a) to solve some RBDO problems related to truss topology optimization. The SML has similarities with multi-point FORM, since in both methods the MPP has to be found and a tangent plane at it is used to locally represent the limit state surface.

Let $\beta(\mathbf{x}) = \Phi^{-1}(\mathbb{P}\{\Omega(\mathbf{x})\})$ the *reliability index* of the design $\mathbf{x}$, where Φ^{-1} stands for the inverse of the standard normal cumulative distribution function. There are two main approaches used in RBDO. In the *reliability index approach* (RIA), the probability constraint is equivalently formulated as $\beta(\mathbf{x}) \geq \Phi^{-1}(1 - P_f)$, which, according to Tu et al. (2001), is the most popular version of the probability constraint. The *performance measure approach* (PMA) considers instead a constraint on the *probabilistic performance measure*, which is computed by an inverse reliability analysis; details can be found in Tu et al. (2001). Both approaches (RIA and PMA) combined with FORM or SORM lead to a double loop iterative procedure, i.e., that one used to find the MPP involved in the reliability assessment is nested into the main iteration of an optimization algorithm. There are, however, many approaches that simplify or totally break the inner loop; we refer the reader to Section 2.2 of Schuëller and Jensen (2008) and Section 1 of Liu et al. (2016a) where detailed lists of references can be found.

In gradient-based optimization algorithms, the sensitivities of the probability constraint function have to be computed. This is done in the case of a single limit state function g by computing the following surface integral:

$$\frac{\partial}{\partial x_i}\mathbb{P}\{\Omega(\mathbf{x})\} = -\int_{\partial\Omega(\mathbf{x})} \frac{f_{\boldsymbol{\xi}}}{\|\nabla_{\boldsymbol{\xi}} g\|}\frac{\partial g}{\partial x_i}\, dS\,. \tag{2}$$

In the case of several limit state functions defined by a vector function $\mathbf{g}$, the expressions can be found in Uryas'ev (1994). When the reliability $\mathbb{P}\{\Omega(\mathbf{x})\}$ is computed by approximating the safe region, such as in FORM and SORM, the integral in (2) is performed on the approximate limit state surface; e.g., the tangent plane at the MPP when FORM is used.

In this paper, we propose a new gradient-based approach to find an approximate solution to (P). The method is of the RIA type, since it involves the direct computation of the failure probability. There are two main ideas behind the proposed method: i) a polytope-like region depending on a vector $\mathbf{s}$ of shape variables is used to approximate the safe region in the random space and ii) the vector $\mathbf{s}$ of shape variables is considered independent of the project variables, and included into the optimization problem.

To fix ideas, let $\Omega(\mathbf{x})$ be the two-dimensional safe region represented in gray in Fig. 1. The polytope-like approximation of the safe region has a boundary defined by a set of vertices $\boldsymbol{\xi}_i$, each one located on a fixed ray starting from the origin. Hence, we have defined a parametric polytope-like region where the shape parameters are the values s_i that represent the distance from the origin to the vertices $\boldsymbol{\xi}_i$. The figure illustrates the case where the points $\boldsymbol{\xi}_i$ are optimally located, i.e., they are on the safe region boundary. However, we emphasize that the shape variables s_i are independent of the project variables, so that the vertices $\boldsymbol{\xi}_i$ are generally inside the safe region, and their optimal location must be found in the optimization process by the optimization algorithm.

There are some immediate advantages of this approach. If the number of shape variables is large enough, then this approach can obtain a better approximation for the safe region than FORM or SORM. The accuracy of the approximation can then be controlled by the user by setting the number of shape variables, enabling the possibility of improving the solution by performing subsequent optimization processes, i.e., a strategy of design based on different optimization stages. Another advantage is that the approximate safe region does not depend on the location of the MPP, so that the proposed method leads naturally to a single loop optimization process. The inclusion of $\mathbf{s}$ into the optimization problem simplifies the sensitivity analysis, since the shape of the approximate shape region will not depend anymore on the design variable $\mathbf{x}$. Hence, the numerical evaluation of expressions such like (2) will not be necessary. However, these advantages can be exploited only if the failure probability, as well as its sensitivities with respect to the vector shape variables $\mathbf{s}$, can be computed easily. We will show that suitable expressions for the failure probability and its sensitivities can be found by viewing the approximate safe region in the space of the generalized spherical coordinates.

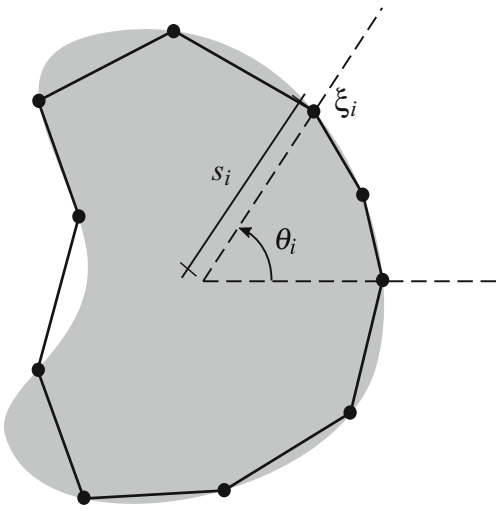

Fig. 1 Approximation of the safe region. Gray: safe region $\Omega(\mathbf{x})$, piecewise linear solid line: boundary of the approximate region $\tilde{\Omega}(\boldsymbol{\xi}_1(\mathbf{s}), \ldots, \boldsymbol{\xi}_k(\mathbf{s}))$ defined by a set of vertices $\boldsymbol{\xi}_i$ located on a fixed ray and at a distance s_i from the origin

The paper layout is as follows. Section 2 describes the proposed procedure of optimization based on a polytope-like approximation of the safe region. Section 3 describes in detail the polytope-like regions used here, which are based on a representation of these regions in the space of the generalized spherical coordinates. The sensitivity analysis is also given in this section. Section 4 presents an application of the proposed method to the topology optimization of truss structures. The simple model of minimizing the total volume of material subject to a probability constraint on the compliance is considered. The numerical results obtained show that the proposed formulation is effective to find a suitable topology. Finally, Section 5 presents the conclusions.

2 Polytope-like approximation of the safe region

The main idea behind the method proposed to find an approximate optimal solution to Problem (P), is to approximate the safe region $\Omega(\mathbf{x})$ by a parametric polytope-like region $\tilde{\Omega}(\boldsymbol{\xi}_1(\mathbf{s}), \ldots, \boldsymbol{\xi}_k(\mathbf{s}))$, where $\boldsymbol{\xi}_1(\mathbf{s}), \ldots, \boldsymbol{\xi}_k(\mathbf{s})$ are control points of the region that depend on the vector of shape variables $\mathbf{s} \in \mathbb{R}^\ell$. To fix ideas, let $\Omega(\mathbf{x})$ be the two-dimensional safe region shown by Fig. 1. A possible approximation $\tilde{\Omega}(\boldsymbol{\xi}_1(\mathbf{s}), \ldots, \boldsymbol{\xi}_k(\mathbf{s}))$ of the safe region could be the polytope shown in the figure, where the control points are the vertices of the polytope, with each one located on a particular ray forming a fixed predefined angle θ_i with respect to the horizontal line. The vector variable $\mathbf{s}$ contains in this example the distances s_i between the control

points and the origin. Note that as more control points are considered, more accurate the approximate region will be. Accuracy could also be improved by considering polytope-like geometries with smooth curved faces instead of flat faces.

The parametric region $\tilde{\Omega}(\boldsymbol{\xi}_1(\mathbf{s}), \ldots, \boldsymbol{\xi}_k(\mathbf{s}))$ should ideally be able to represent exactly the safe region $\Omega(\mathbf{x})$. More precisely, assume that $\tilde{\Omega}(\boldsymbol{\xi}_1(\mathbf{s}), \ldots, \boldsymbol{\xi}_k(\mathbf{s}))$ satisfies the following assumptions:

i) If $\mathbf{g}(\mathbf{x}, \boldsymbol{\xi}_i(\mathbf{s})) \leq 0$ for $i = 1, \ldots, k$, then $\tilde{\Omega}(\boldsymbol{\xi}_1(\mathbf{s}), \ldots, \boldsymbol{\xi}_k(\mathbf{s})) \subset \Omega(\mathbf{x})$.
ii) For all $\mathbf{x}$ satisfying $\mathbf{h}(\mathbf{x}) \leq 0$, there is $\mathbf{s} \in \mathbb{R}^{\ell}$, such that $\mathbf{g}(\mathbf{x}, \boldsymbol{\xi}_i(\mathbf{s})) \leq 0$, for $i = 1, \ldots, k$, and $\tilde{\Omega}(\boldsymbol{\xi}_1(\mathbf{s}), \ldots, \boldsymbol{\xi}_k(\mathbf{s})) \equiv \Omega(\mathbf{x})$.

Then, the next theorem shows that we can find an optimal solution to Problem (P) by considering a different optimization problem that considers instead a probability constraint on the parametric region $\tilde{\Omega}(\boldsymbol{\xi}_1(\mathbf{s}), \ldots, \boldsymbol{\xi}_k(\mathbf{s}))$:

Theorem 1 *Suppose that $\tilde{\Omega}(\boldsymbol{\xi}_1(\mathbf{s}), \ldots, \boldsymbol{\xi}_k(\mathbf{s}))$ is a parametric region that satisfies assumptions i) and ii) above. Then, the optimal solution $(\mathbf{x}^*, \mathbf{s}^*)$ to the following problem:*

$$
\begin{aligned}
&\min_{\mathbf{x},\mathbf{s}} f(\mathbf{x}) \,, \\
&s.t.\ \mathbf{g}(\mathbf{x}, \boldsymbol{\xi}_i(\mathbf{s})) \leq 0, \quad for\ i = 1, \ldots, k \,, \qquad (P_A) \\
&\mathbb{P}\{\tilde{\Omega}(\boldsymbol{\xi}_1(\mathbf{s}), \ldots, \boldsymbol{\xi}_k(\mathbf{s}))\} \geq 1 - P_f \,, \\
&\mathbf{h}(\mathbf{x}) \leq 0 \,,
\end{aligned}
$$

provides an optimal solution $\mathbf{x}^*$ for Problem (P).

Proof Note that if $\mathbf{x}^*$ is an optimal solution of Problem (P), then by assumption ii), there is $\mathbf{s}^*$ such that $(\mathbf{x}^*, \mathbf{s}^*)$ is feasible for Problem (P_A). Moreover, if $(\mathbf{x}^*, \mathbf{s}^*)$ is an optimal solution to Problem (P_A), then by assumption i) $\mathbf{x}^*$ is feasible for Problem (P). Both of them are then equivalent in terms of the design variable $\mathbf{x}$. □

Note that both assumptions i) and ii) are quite strong and hard to satisfy in a practical application. For instance, Fig. 1 shows the case that both assumptions are violated: the inclusion $\tilde{\Omega}(\boldsymbol{\xi}_1(\mathbf{s}), \ldots, \boldsymbol{\xi}_k(\mathbf{s})) \subset \Omega(\mathbf{x})$ of assumption i) is not true, and it is impossible to choose $\mathbf{s}$ in order to obtain $\tilde{\Omega}(\boldsymbol{\xi}_1(\mathbf{s}), \ldots, \boldsymbol{\xi}_k(\mathbf{s})) \equiv \Omega(\mathbf{x})$ as assumption ii) demands. However, both of them can be satisfied in an approximate sense by considering a large number of control points.

The following comments may be useful to understand why problem (P_A) leads to an optimal solution to problem (P). Note that the project variable $\mathbf{x}$ and the shape variable $\mathbf{s}$ are independent variables of problem (P_A). The objective function $f(\mathbf{x})$ and the safe region $\Omega(\mathbf{x})$ (gray region in Fig. 1) depend on the project variable $\mathbf{x}$. Then, by changing the variable $\mathbf{x}$ the optimization algorithm changes the value of the objective function and the shape of the safe region simultaneously. The polytope-like region $\tilde{\Omega}(\boldsymbol{\xi}_1(\mathbf{s}), \ldots, \boldsymbol{\xi}_k(\mathbf{s}))$ depends only on the shape variable $\mathbf{s}$. Then by changing $\mathbf{s}$ the optimization algorithm changes the shape of the polytope. However, the optimization algorithm must respect the constraints $\mathbf{g}(\mathbf{x}, \boldsymbol{\xi}_i(\mathbf{s})) \leq 0$, which basically means that the vertices $\boldsymbol{\xi}_i(\mathbf{s})$ of the polytope must be inside the safe region. Roughly speaking, at each feasible design $(\mathbf{x}, \mathbf{s})$, the polytope $\tilde{\Omega}(\boldsymbol{\xi}_1(\mathbf{s}), \ldots, \boldsymbol{\xi}_k(\mathbf{s}))$ is contained by the safe region $\Omega(\mathbf{x})$. Suppose that the optimization algorithm starts at a feasible design $(\mathbf{x}, \mathbf{s})$, i.e., the polytope is contained by the safe region (maybe strictly contained), and the probability $\mathbb{P}\{\tilde{\Omega}(\boldsymbol{\xi}_1(\mathbf{s}), \ldots, \boldsymbol{\xi}_k(\mathbf{s}))\}$ is above the specified lower bound. In the optimization process, the optimization algorithm will try to change the project variable $\mathbf{x}$ in order to reduce the value of the objective function $f(\mathbf{x})$, i.e., to obtain cheaper designs. However, cheaper designs are more likely to fail, i.e., the cheaper the design, the smaller the safe region $\Omega(\mathbf{x})$. Therefore, in the optimization process, cheaper designs will be found for which the size of the safe region $\Omega(\mathbf{x})$ is progressively reduced. Since the size of the polytope $\tilde{\Omega}(\boldsymbol{\xi}_1(\mathbf{s}), \ldots, \boldsymbol{\xi}_k(\mathbf{s}))$ cannot be arbitrarily reduced (due to the probability constraint), the boundary $\partial\Omega(\mathbf{x})$ of the safe region will eventually come into contact with the boundary of a polytope of minimum possible size. In that situation, the optimization process must end, since the optimization algorithm cannot find a cheaper feasible design without producing a violation of the probability constraint. Note that only the final polytope approximates the safe region (polytopes of intermediate iterations may not approximate the corresponding safe regions); hence, the approximation of the safe region is built throughout the optimization process for the optimal design only. This is a different approach from other classical methods such like FORM and SORM, where the approximate region is built for each evaluation of the probability constraint.

Note that Problem (P_A) looks quite suitable for finding an approximate optimal solution. First, it has a set of deterministic constraints $\mathbf{g}(\mathbf{x}, \boldsymbol{\xi}_i(\mathbf{s})) \leq 0$, that are not challenging from the point of view of the function evaluation and sensitivity analysis (all the tools developed for deterministic problems should be appropriate), and only one probabilistic constraint that does not depend on the design variable $\mathbf{x}$. The probabilistic constraint depends only on the shape variables $\mathbf{s}$, and this dependency is quite direct. In the following sections, we will show some appropriate numerical techniques for the evaluation of the probability constraint, as well as its functional derivatives. Second, since the shape variables $\mathbf{s}$ of the polytope $\tilde{\Omega}(\boldsymbol{\xi}_1(\mathbf{s}), \ldots, \boldsymbol{\xi}_k(\mathbf{s}))$ are added to the optimization problem, then the optimization process will find simultaneously the

optimal solution and the approximate safe region, without implying nested iterations such like e.g. in FORM-based RDBO, where the approximation of the safe region implies itself an iterative process to find the MPP. Third, differently from other techniques such like FORM-based methods, the one proposed has the advantage of allowing the user to control the accuracy of the probability estimation. The user could in principle obtain solutions with arbitrary accuracy by increasing the number of control points. Of course, as more control points are used, more time-consuming will be the optimization process. Anyway, the proposed method allows the possibility of reaching a suitable design by considering different levels of accuracy in different stages.

To illustrate the ideas mentioned above, we consider the following problem:

$$\begin{aligned} \min_x f(x) &= x\,, \\ \text{s.t. } \mathbb{P}\{\Omega(x)\} &\geq 1 - P_f\,, \\ x &\geq 0\,, \end{aligned}$$

where $\Omega(x) = \{|\xi| \leq x\}$ and ξ is a univariate normal random variable of zero mean and unitary variance. Note that, for $x > 0$, $\Omega(x) = [-x, x]$, hence $\mathbb{P}\{\Omega(x)\} = \Phi(x) - \Phi(-x) = 1 - 2\Phi(-x)$. Then, the probability constraint can be rewritten as $x \geq -\Phi^{-1}(P_f/2)$. The optimal solution is then $x^* = -\Phi^{-1}(P_f/2)$ provided $0 < P_f \leq 1$.

Since the random space is one-dimensional, the natural approximation of the safe region is an interval given by two control points: $\tilde{\Omega}(\xi_1(\mathbf{s}), \xi_2(\mathbf{s})) = [\xi_1(\mathbf{s}), \xi_2(\mathbf{s})]$, where the control points are given by $\xi_1(\mathbf{s}) = -s_1$, $\xi_2(\mathbf{s}) = s_2$, i.e., the first control point is in the ray $(-\infty, 0]$ at a distance s_1 from the origin, and the second one is in the ray $[0, \infty)$ at a distance s_2, being s_1 and s_2 the two positive shape variables of the parametric interval. The approximate version (P_A) of the example is then given by

$$\begin{aligned} \min_{x,\mathbf{s}} f(x) &= x\,, \\ \text{s.t. } s_1 &\leq x\,, \\ s_2 &\leq x\,, \\ \mathbb{P}\{[-s_1, s_2]\} &\geq 1 - P_f\,, \\ x &\geq 0\,. \end{aligned}$$

Note that the approximate version has two additional variables and two additional constraints. We emphasize that the additional variables s_1 and s_2 are independent of x, which means that the probability constraint no longer depends on x, and that the safe region $\Omega(x)$ and the interval $\tilde{\Omega}(\xi_1(\mathbf{s}), \xi_2(\mathbf{s}))$ are not related in principle. However, each feasible triplet (x, s_1, s_2) satisfies $s_1 \leq x$ and $s_2 \leq x$, which gives $\tilde{\Omega}(\xi_1(\mathbf{s}), \xi_2(\mathbf{s})) \subset \Omega(x)$, and assumption i) of Theorem 1 holds. By taking $s_1 = s_2 = x$, we see that assumption ii) holds also. Then, by Theorem 1 we have that the approximate version must provide the exact solution. In fact, $\mathbb{P}\{[-s_1, s_2]\} = \Phi(s_2) - \Phi(-s_1) = 1 - \Phi(-s_1) - \Phi(-s_2)$, and since $s_i \leq x$, then $\Phi(-s_i) \geq \Phi(-x)$. Therefore, the first three constraints of the approximate problem imply $x \geq -\Phi^{-1}(P_f/2)$. The optimal solution is then given by the feasible triplet (x^*, x^*, x^*) with $x^* = -\Phi^{-1}(P_f/2)$.

We end this section by showing several toy examples that will be useful to understand how the proposed method works in more realistic situations. In particular, we will discuss the effect that the non-satisfaction of assumptions i) and ii) has on the approximate optimal designs. The toy examples are related to the optimization of truss structures, and we will proceed to discuss the results obtained without giving details about the problems considered, such as the computation of performance functions and probability constraint. Details about the computation of the probability constraint and its derivatives are given in Section 3, and details about the design of truss structures are given in Section 4. All the toy examples are solved using the quasi-Newton, interior-point algorithm FAIPA (Herskovits et al. 2005) provided with first order sensitivities of the performance functions.

The first example is depicted in Fig. 2. The design variables of the example are the cross-section areas of the bars, which are considered deterministic, the objective function is the total volume of the structure and the limit state function is $g(\mathbf{x}, \boldsymbol{\xi}) = c(\mathbf{x}, \boldsymbol{\xi}) - c_0$, where $c(\mathbf{x}, \boldsymbol{\xi})$ is the compliance of the structure and $c_0 = 1\,\text{Nm}$. The deterministic constraint is $\mathbf{x} \geq 0$, and the failure probability $P_f = 1.35 \times 10^{-3}$ which corresponds to the reliability index $\beta = 3$. The approximate safe region is defined following

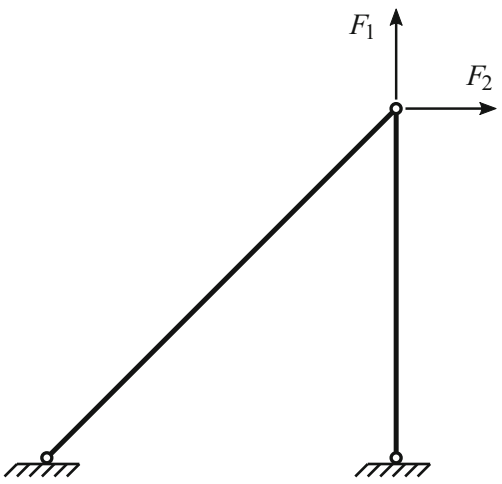

Fig. 2 First toy example. The bars have lengths $\sqrt{2}\,\text{m}$ and 1 m, and they are composed by a linear elastic material with Young's modulus $E = 1\,\text{Pa}$. The forces F_1 and F_2 are of 1 N of magnitude. The random loading is $\xi_1 F_1 + 0.1\xi_2 F_2$, where the pair (ξ_1, ξ_2) is a multivariate normal random variable with zero mean and identity covariance matrix

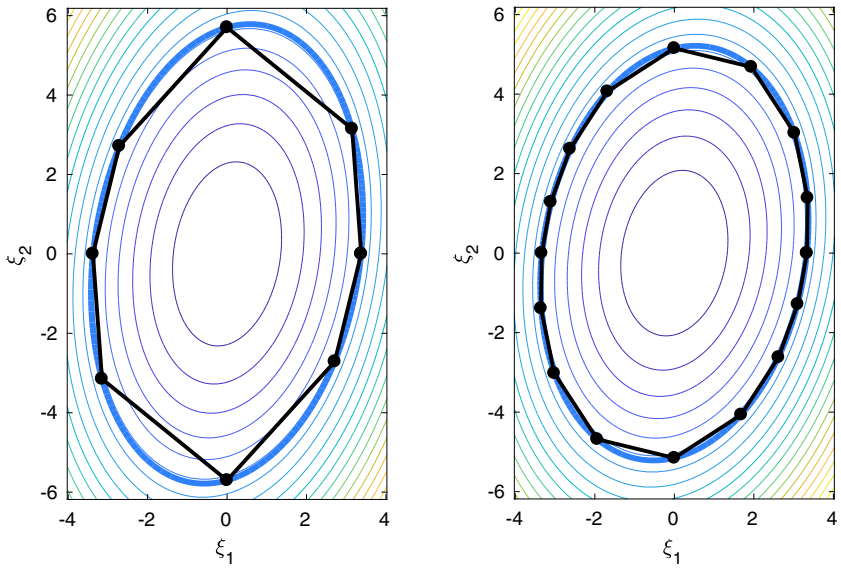

Fig. 3 First toy example: safe regions and their approximate counterparts in the final design when considering 8 and 16 control points. The figures show some contour levels of the compliance function. The thick contour line corresponds to the level c_0

the idea of Fig. 1, considering rays that divide the plane in equal angles.

When we solved Problem (P_A) considering 8 control points, we obtained an optimized structure of 12.75 m^3 of material, while when considering 16 control points the total amount of material is 12.21 m^3. Figure 3 shows the safe region $\Omega(\mathbf{x})$ for the final design and its corresponding approximate $\tilde{\Omega}(\boldsymbol{\xi}_1(\mathbf{s}), \ldots, \boldsymbol{\xi}_k(\mathbf{s}))$. Note in the figure that the safe regions are convex in this example, a consequence of the fact that the compliance is a convex function with respect to the load values. Therefore, the approximate region is entirely inside the real safe region, which means that assumption i) is satisfied, and the failure probability is overestimated. The optimized designs have then a reliability index higher than the target one: $\beta = 3.091$ when using 8 control points, and $\beta = 3.025$ when using 16 control points (the final values of the reliability index are computed by considering approximate regions with a high number of control points, following the same evaluation techniques presented in Section 3). Since assumption ii) is not satisfied, the solutions obtained are not exact. However, by increasing the number of control points a lighter structure is obtained with a reliability index closer to the target value. Figure 3 shows also the advantage of considering rays forming equal angles. The line segments of the piecewise boundary of the approximate region are smaller in the regions of the boundary closer to the origin. Hence, a better fitting of the failure surface is obtained in a neighborhood of the MPP.

The second example is the same of Fig. 2, but in this case the random load is $F_1 + 0.1\xi_1 F_2$, and the inclined bar has a cross-section area that is now considered random of value $x_1 + A\xi_2$, with $A = 0.1\,m^2$. The pair (ξ_1, ξ_2) is a

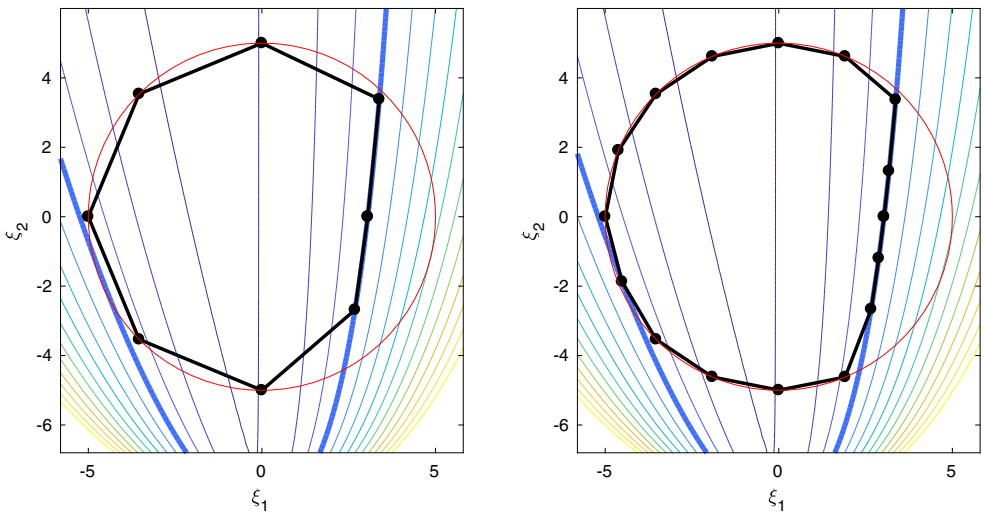

Fig. 4 Second toy example: safe regions and their approximate counterparts in the final design when considering 8 and 16 control points. The figures show some contour levels of the compliance function. The thick contour line corresponds to the level c_0, and the thin red line indicates the maximum possible value for the shape variables s_i

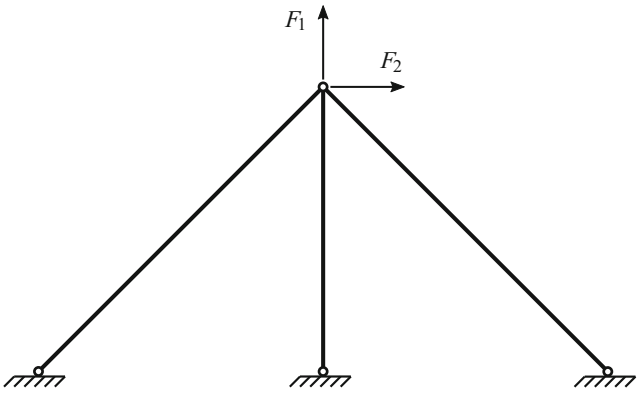

Fig. 5 Third toy example. The bars have lengths $\sqrt{2}$ m, 1 m and and $\sqrt{2}$ m, and are composed by a linear elastic material with Young's modulus $E = 1$ Pa. The forces F_1 and F_2 are of 1 N of magnitude. The random loading is $F_1 + 0.1\xi_1 F_2$, and the inclined bar on the left has a cross-section area that is $x_1 + A\xi_2$, with $A = 0.1\,\text{m}^2$. The pair (ξ_1, ξ_2) is a multivariate normal random variable with zero mean and identity covariance matrix

multivariate normal random variable with zero mean and identity covariance matrix. In this example, two limit state functions are considered; one related to the compliance: $g_1(\mathbf{x}, \boldsymbol{\xi}) = c(\mathbf{x}, \boldsymbol{\xi}) - c_0$ with $c_0 = 1\,\text{Nm}$, and the other one related to the cross-section area of the inclined bar: $g_2(\mathbf{x}, \boldsymbol{\xi}) = -x_1 - A\xi_2$. In this example, the safe region $\Omega(\mathbf{x})$ is still convex, since the compliance is a convex function with respect to the load values and the cross-section areas. However, in this case, the safe region is unbounded. In order to obtain convergence to a solution, we have set a finite upper bound on the variables s_i, i.e., each variable s_i is sought in the interval $[0, s_0]$ with $s_0 = 5$. Note that this upper bound is an additional source of error in the computation of the failure probability. However, it prevents the control points to go through a region of quite low probability, so that the error introduced is actually rather small. When using 8 control points, we obtained a structure of $3.669\,\text{m}^3$ with $\beta = 3.022$, while when using 16 control points, we obtained a structure of $3.649\,\text{m}^3$ with $\beta = 3.004$. The safe regions of the optimized designs are shown in Fig. 4.

As a third toy example we consider the truss of Fig. 5, which is the same of the second example but with an additional inclined bar with deterministic cross-section area on the right. Two limit state functions are considered; one related to the vertical displacement of the free node: $g_1(\mathbf{x}, \boldsymbol{\xi}) = u_0 - u_1(\mathbf{x}, \boldsymbol{\xi})$ where $u(\mathbf{x}, \boldsymbol{\xi})$ is the vertical displacement and $u_0 = -0.4\,\text{m}$, and the other one related to the cross-section area of the inclined bar on the left: $g_2(\mathbf{x}, \boldsymbol{\xi}) = -x_1 - A\xi_2$. In this example, the safe region is nonconvex and unbounded. As in the second example, each variable s_i is sought in the interval $[0, s_0]$ with $s_0 = 5$. When using 8 control points, we obtained an optimized structure of $3.363\,\text{m}^3$ of material with $\beta = 2.973$, while when using 16 control points the total amount of material is $3.366\,\text{m}^3$ and $\beta = 2.999$. Figure 6 shows the safe region $\Omega(\mathbf{x})$ for the final design and its corresponding approximate $\tilde{\Omega}(\boldsymbol{\xi}_1(\mathbf{s}), \ldots, \boldsymbol{\xi}_k(\mathbf{s}))$. Since in this example the safe region is nonconvex, the assumption i) is not satisfied, and the failure probability can be underestimated. That is the reason why the solution with 16 control points is heavier and safer than the solution with 8 control points.

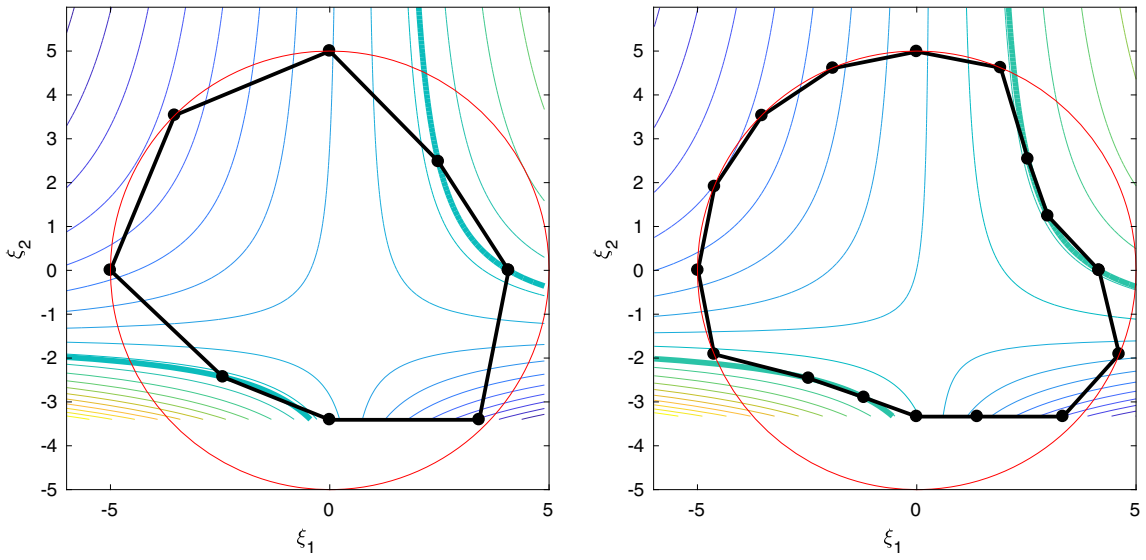

Fig. 6 Third toy example: safe regions and their approximate counterparts in the final design when considering 8 and 16 control points. The figures show some contour levels of the vertical displacement which are drawn only in the region satisfying $g_2(\mathbf{x}, \boldsymbol{\xi}) \leq 0$. The thick contour line corresponds to the level u_0, and the thin red line indicates the maximum possible value for the shape variables s_i

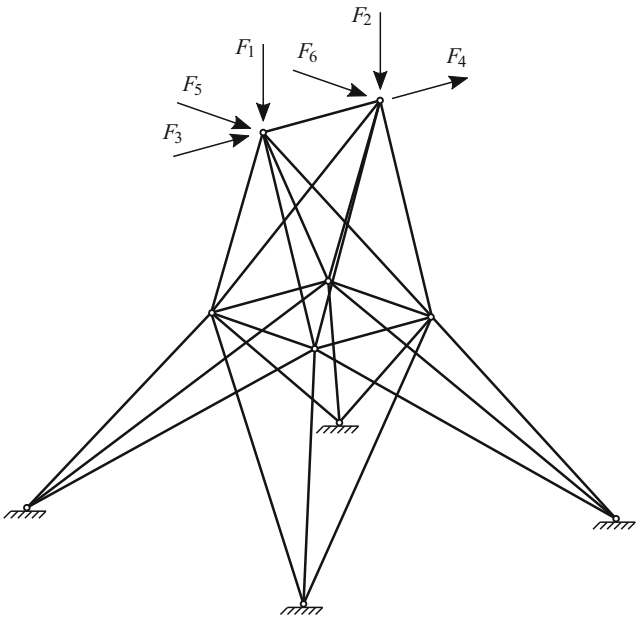

Fig. 7 Fourth toy example. The bars are composed by a linear elastic material with Young's modulus $E = 1$ Pa. The forces F_1–F_6 are all of 1 N of magnitude. Let $\mathbf{f}_0 = F_1 + F_2$, $\mathbf{f}_1 = F_3 + F_4$, $\mathbf{f}_2 = F_5 + F_6$, $\mathbf{f}_3 = F_5 - F_6$. Then, the random loading is $\mathbf{f}_0 + 0.1\xi_1\mathbf{f}_1 + 0.1\xi_2\mathbf{f}_2 + 0.1\xi_3\mathbf{f}_3$, where (ξ_1, ξ_2, ξ_2) is a multivariate normal random variable of zero mean and identity covariance matrix

The fourth example consists of a three-dimensional truss submitted to the random loads detailed in Fig. 7. For the geometry of this example see (Canelas et al. 2017). The bar areas are considered deterministic, while the loading is random. The limit state function is the compliance $g(\mathbf{x}, \boldsymbol{\xi}) = c(\mathbf{x}, \boldsymbol{\xi}) - c_0$ with $c_0 = 2.168$ Nm, which corresponds to the compliance of the design of unitary cross-sectional areas when submitted to the mean load. In this case, a safe region in a three-dimensional random space has to be approximated. Such as in the previous examples, the control points are located on fixed rays, each one corresponding to a point of a regular grid defined on the space of the angular variables of the usual spherical coordinates. The safe regions found for two different meshes are depicted in Fig. 8. When using the mesh of 4×8 faces for the failure region a truss of 53.32 m^3 is obtained, with a reliability $\beta = 3.397$. When the mesh has 8×16 faces the volume obtained is 49.57 m^3 and the reliability is $\beta = 3.091$.

3 Evaluation of the probability constraint

In the previous section, it was shown that the strategy of Fig. 1 can be used successfully to solve some examples in a two-dimensional random space. In this section, we show how to extend the idea of Fig. 1 to higher-dimensional random spaces, and how to compute the failure probability and its derivatives with reasonable accuracy. We will assume that the polytope-like region $\tilde{\Omega}(\boldsymbol{\xi}_1(\mathbf{s}), \ldots, \boldsymbol{\xi}_k(\mathbf{s}))$ is star-shaped with respect to the origin. Note that the safe region is not generally star-shaped, for instance when it is composed by a set of unconnected domains. If the safe region is not star-shaped, then the polytope can approximate only the set of points of the safe region that are "visible" from the origin. Hence, the probability of failure will be overestimated in the case of safe regions that are not star-shaped (see Fig. 9).

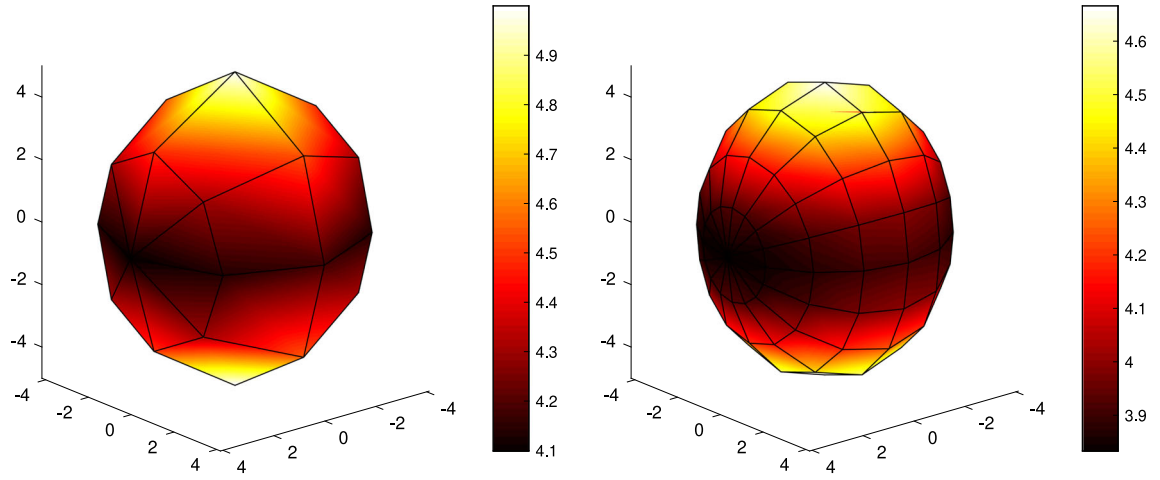

Fig. 8 Fourth toy example: safe regions of the final design when considering 4×8 and 8×16 faces. The color indicates the distance from the origin to the approximate limit state surface

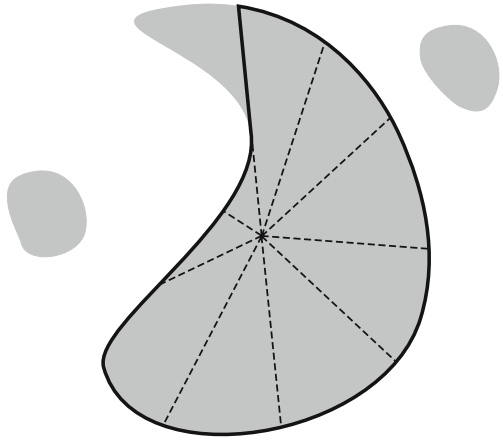

Fig. 9 Approximation of a safe region that is not star-shaped. The safe region $\Omega(\mathbf{x})$ is represented in gray and is composed of three unconnected components. The best star-shaped approximation is bounded by the thick black solid line. Note that only part of the connected region containing the origin is considered in the approximation (the points that are "visible" from the origin). Hence, the failure probability is overestimated

The main idea proposed here is to view the safe region in the space of generalized spherical coordinates. In an n-dimensional space, these coordinates are defined by

$$\begin{aligned}
\xi_1 &= r\cos(\theta_1)\,,\\
\xi_2 &= r\sin(\theta_1)\cos(\theta_2)\,,\\
\xi_3 &= r\sin(\theta_1)\sin(\theta_2)\cos(\theta_3)\,,\\
&\vdots\\
\xi_{n-1} &= r\sin(\theta_1)\ldots\sin(\theta_{n-2})\cos(\theta_{n-1}),\\
\xi_n &= r\sin(\theta_1)\ldots\sin(\theta_{n-2})\sin(\theta_{n-1}).
\end{aligned}$$

Let $\boldsymbol{\theta} = (\theta_1, \ldots, \theta_{n-1})$, and $\Theta = [0, \pi] \times \cdots \times [0, \pi] \times [0, 2\pi]$. Since the polytope is assumed star-shaped, then it is the following set in the space of the generalized spherical coordinates:

$$\tilde{\Omega}'(\boldsymbol{\xi}_1(\mathbf{s}), \ldots, \boldsymbol{\xi}_k(\mathbf{s})) = \{(r, \boldsymbol{\theta}) : \boldsymbol{\theta} \in \Theta\,, \text{ and } r \in [0, R(\mathbf{s}, \boldsymbol{\theta})]\}\,, \quad (3)$$

where $R(\mathbf{s}, \boldsymbol{\theta})$ is the distance from the origin to the boundary $\partial\tilde{\Omega}(\boldsymbol{\xi}_1(\mathbf{s}), \ldots, \boldsymbol{\xi}_k(\mathbf{s}))$ of the polytope in the direction given by $\boldsymbol{\theta}$.

For instance, the two-dimensional safe region of Fig. 1 is shown in the space of the generalized spherical coordinates in Fig. 10. Note that the piecewise linear boundary of Fig. 1 means a piecewise nonlinear boundary of $\tilde{\Omega}'(\boldsymbol{\xi}_1(\mathbf{s}), \ldots, \boldsymbol{\xi}_k(\mathbf{s}))$. Of course, one could consider a piecewise linear boundary for $\tilde{\Omega}'(\boldsymbol{\xi}_1(\mathbf{s}), \ldots, \boldsymbol{\xi}_k(\mathbf{s}))$, and in this case, the original domain $\tilde{\Omega}(\boldsymbol{\xi}_1(\mathbf{s}), \ldots, \boldsymbol{\xi}_k(\mathbf{s}))$ would be a polytope-like region limited by smooth curved faces.

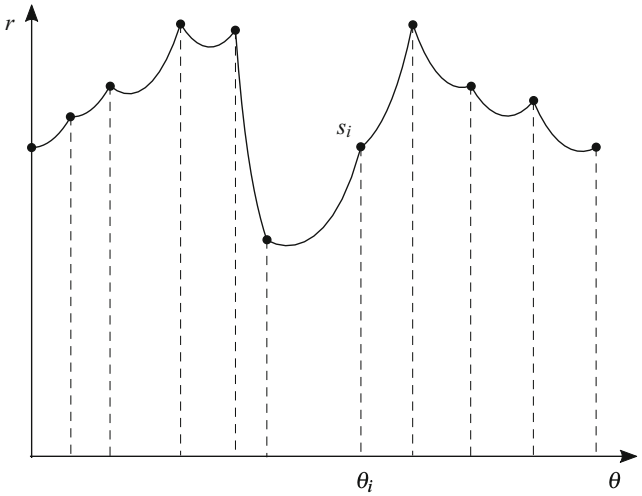

Fig. 10 Safe region $\tilde{\Omega}'(\boldsymbol{\xi}_1(\mathbf{s}), \ldots, \boldsymbol{\xi}_k(\mathbf{s}))$ in the space of the generalized spherical coordinates

Let $P_f(\mathbf{s})$ be the failure probability given by $P_f(\mathbf{s}) = 1 - \mathbb{P}\{\tilde{\Omega}(\boldsymbol{\xi}_1(\mathbf{s}), \ldots, \boldsymbol{\xi}_k(\mathbf{s}))\}$. It can be computed by integrating the density function corresponding to the probability distribution in the *unsafe region* $\mathbb{R}^n \setminus \tilde{\Omega}(\boldsymbol{\xi}_1(\mathbf{s}), \ldots, \boldsymbol{\xi}_k(\mathbf{s}))$. The change of variables of the generalized spherical coordinates and the Fubini theorem provide:

$$P_f(\mathbf{s}) = \int_{R(\mathbf{s},\boldsymbol{\theta})}^{+\infty} \int_{\Theta} J(r, \boldsymbol{\theta})\, f_n(r, \boldsymbol{\theta})\, d\boldsymbol{\theta}\, dr\,, \quad (4)$$

where $J(r, \boldsymbol{\theta})$ is the Jacobian determinant of the transformation and $f_n(r, \boldsymbol{\theta})$ is the probability density function. In the case of a multivariate normal random variable of zero mean and identity covariant matrix, we have

$$\begin{aligned}
J(r, \boldsymbol{\theta}) &= r^{n-1} S(\boldsymbol{\theta}),\\
S(\boldsymbol{\theta}) &= \sin^{n-2}(\theta_1)\sin^{n-3}(\theta_2)\ldots\sin(\theta_{n-2}),\\
f_n(r, \boldsymbol{\theta}) &= (2\pi)^{-n/2}\exp(-r^2/2).
\end{aligned}$$

Hence, (4) becomes

$$P_f(\mathbf{s}) = \int_{\Theta} S(\boldsymbol{\theta})\, F_n(\mathbf{s}, \boldsymbol{\theta})\, d\boldsymbol{\theta}\,, \quad (5)$$

where the function $F_n(\mathbf{s}, \boldsymbol{\theta})$ is given by

$$F_n(\mathbf{s}, \boldsymbol{\theta}) = \int_{R(\mathbf{s},\boldsymbol{\theta})}^{+\infty} (2\pi)^{-n/2} r^{n-1} \exp(-r^2/2)\, dr\,. \quad (6)$$

We observe that closed expressions in terms of known functions can be found for $F_n(\mathbf{s}, \boldsymbol{\theta})$. They are given by the

expressions obtained for $n = 1; 2$, and a recurrence relation which can be found through integration by parts:

$$\begin{aligned} n = 1: \quad & F_1(\mathbf{s}, \boldsymbol{\theta}) = 1 - \Phi(R(\mathbf{s}, \boldsymbol{\theta})), \\ n = 2: \quad & F_2(\mathbf{s}, \boldsymbol{\theta}) = (2\pi)^{-1} \exp\left(-R(\mathbf{s}, \boldsymbol{\theta})^2/2\right), \\ n > 2: \quad & F_n(\mathbf{s}, \boldsymbol{\theta}) = (2\pi)^{-(n-2)/2} R(\boldsymbol{\theta})^{n-2} F_2(\mathbf{s}, \boldsymbol{\theta}) \\ & \quad + (n-2)(2\pi)^{-1} F_{n-2}(\mathbf{s}, \boldsymbol{\theta}). \end{aligned}$$

We are now in the position to explain the advantages of using generalized spherical coordinates. In the first place, they allow the expression (5) for the failure probability. The domain of integration Θ is a rectangular box that can be divided into a regular mesh of squares (cubes and hyper-cubes in higher-dimensional spaces) which is quite convenient for numerical quadrature. The second advantage is that the regular mesh used defines the rays in the original probability space where the vertices of the polytope are located. In fact, the polytope-like region used to approximate the safe region is first defined in the space of generalized spherical coordinates.

Many schemes of integration can be used to compute (5). Consider for instance the two-dimensional example of Fig. 10 defined by a grid of k intervals. In this case $S(\boldsymbol{\theta}) = 1$, and the trapezoidal rule applied to (5) provides:

$$P_f(\mathbf{s}) \approx \sum_{i=1}^{k} \frac{\theta_2^i - \theta_1^i}{2} \left[S(\theta_1^i) F_n(\mathbf{s}, \theta_1^i) + S(\theta_2^i) F_n(\mathbf{s}, \theta_2^i) \right], \tag{7}$$

where θ_1^i and θ_2^i are the limits of the i-th interval. The previous result is in fact exact for the probability of the approximate safe region if it is defined by a piecewise linear boundary in the space of the generalized spherical coordinates. If other interpolation schemes are used, then more elaborated schemes of integration can be used, e.g., the Gauss quadrature. For instance, in the toy examples of Section 2, the approximate safe regions of Figs. 3, 4, 5, and 6 were assumed limited by linear faces, so that, $R(\mathbf{s}, \boldsymbol{\theta})$ was piecewise nonlinear such as in Fig. 10. The procedure used for obtaining the accurate results presented was to divide each interval $[\theta_1^i, \theta_2^i]$ into three subintervals before the application of the trapezoidal rule.

If the random space has dimension $n > 2$, then the above ideas can be extended easily. Since Θ has a rather simple geometry, we can divide it in squares, cubes, hyper-cubes, etc., interpolating the nodal values of $R(\mathbf{s}, \boldsymbol{\theta})$ and using a simple scheme of integration to obtain a sum such as (7).

The sensitivities of the failure probability can be computed quite easily as well. Consider for instance the failure probability given by (7). Then, we have

$$\frac{\partial P_f}{\partial s_j}(\mathbf{s}) \approx \sum_{i=1}^{k} \frac{\theta_2^i - \theta_1^i}{2} \left[S(\theta_1^i) \frac{\partial F_n}{\partial s_j}(\mathbf{s}, \theta_1^i) + S(\theta_2^i) \frac{\partial F_n}{\partial s_j}(\mathbf{s}, \theta_2^i) \right]. \tag{8}$$

Note that the partial derivatives are zero when the angles θ_1^i and θ_2^i are not the angle θ_j corresponding to the j-th node. For the angle θ_j, since $R(\mathbf{s}, \theta_j) = s_j$, by differentiating (6) we obtain

$$\frac{\partial F_n}{\partial s_j}(\mathbf{s}, \theta_j) = -(2\pi)^{-n/2} s_j^{n-1} \exp(-s_j^2/2). \tag{9}$$

Derivatives of higher order can be easily obtained by differentiating (8) and (9).

Although the formulation presented is general, we note that a regular mesh for $\Theta = [0, \pi] \times \cdots \times [0, \pi] \times [0, 2\pi]$ leads to a large number of control points in the case of high-dimensional random spaces. For instance, a mesh of $d \times d \times \cdots \times d \times 2d$ intervals define approximately $2(d+1)^{n-1}$ control points. By taking $d = 4$, we obtain 10, 250, 6250, and 156250 control points for $n = 2$, 4, 6, 8, respectively. Hence, an accurate representation of the safe region is possible only in the case of low-dimensional random spaces.

The dimension n of the random space can also affect the accuracy of the failure probability computed. To see this, we considered a safe region with the shape of a ball of radius $r = 3$ centered at the point $\boldsymbol{\xi} = (1, 0, \ldots, 0)$. The ball was approximated by a polytope with vertices located on the spherical failure surface. For the polytope we considered regular meshes with $d = 4$, 6, 8, 10 and 12. To compute the failure probability each of the $d \times d \times \cdots \times d \times 2d$ hyper-cubes of the mesh was divided into $3 \times 3 \times \cdots \times 3$ elements, and the integration of the failure probability in the elements was obtained by Gaussian quadrature with only one integration point. Table 1 provides the results obtained for the polytopes considered and also by using FORM. The probability computed by using FORM is actually the same independently of the dimension of the space considered, since it corresponds to the probability of the half space $\xi_1 \leq -2$, i.e., the value $\Phi(-2) = 2.275 \times 10^{-2}$. Table 1 shows that the polytope method tends to overestimate the failure probability (the polytope is contained by the safe region), and shows that a value $d \approx 2n$ is required to keep the error of the reliability index below 10 % (highlighted figures in the table). FORM instead tends to underestimate

Table 1 Values of $\bar{P}_f/P_f$ and $\bar{\beta}/\beta$, i.e., computed values over reference ones

Mesh	$n = 1$	$n = 2$	$n = 3$	$n = 4$	$n = 5$
$d = 4$	*1.000, 1.000*	*1.219, 0.944*	1.458, 0.852	1.642, 0.718	1.748, 0.508
$d = 6$	1.000, 1.000	1.090, 0.976	*1.182, 0.936*	1.255, 0.877	1.306, 0.781
$d = 8$	1.000, 1.000	1.049, 0.987	1.097, 0.965	*1.136, 0.932*	1.164, 0.878
$d = 10$	1.000, 1.000	1.030, 0.992	1.060, 0.978	1.084, 0.957	*1.102, 0.923*
$d = 12$	1.000, 1.000	1.021, 0.994	1.041, 0.985	1.057, 0.971	1.069, 0.948
FORM	0.999, 1.000	0.520, 1.171	0.296, 1.402	0.183, 1.732	0.122, 2.240

Notations: $\bar{P}_f$: failure probability computed with the polytope or with FORM, P_f: reference value, $\bar{\beta}$: reliability index computed, β: reference value, n: dimension of the random space. Reference values are numerically computed by using a polytope with $d = 50$. The highlighted figures indicate the smaller value d for which the error of β is less than 10 %

the failure probability, and for the ball considered the error can be quite significant even for the dimension $n = 2$.

4 Topology optimization of truss structures

Trusses are two or three-dimensional mechanical structures that consist of an ensemble of L nodes joint by m bars, which are made of a linear elastic, isotropic and homogeneous material. Trusses are designed to support one or more external *loadings*, each one consisting of one or more forces applied to the nodes of the structure, see e.g. (Achtziger 1997; Bendsøe 1995). In the so-called ground structure approach (Dorn et al. 1964), nodal positions are fixed in the reference configuration, and the optimal truss structure is found by considering only bar volumes as design variables. When a mesh full of nodes and bars is considered, which is referred to as the ground structure, a suitable geometry can be found as a strict subset, hence simulating the effect of geometric variables. The high number of nodes and potential bars made these problems typically large scale. The large size of the typical problems requires that the solution be found by using specific algorithms applied to special reformulations of the compliance optimization model, see e.g. (Makrodimopoulos et al. 2009). Suitable practical designs are usually found, since a large number of potential bar volumes vanishes at the optimum.

Let us consider first the deterministic model related to the topology optimization of trusses. A largely employed model consists of minimizing the total volume of material subject to a constraint on the compliance:

$$\begin{aligned} &\min_{\mathbf{x}} \sum_{i=1}^{m} \ell_i x_i \,, \\ &\text{s.t. } c(\mathbf{x}) \le c_0 \,, \qquad (P_D) \\ &\mathbf{x} \ge 0 \,, \end{aligned}$$

where $\mathbf{x}$ is the vector of cross-sectional areas of the bars, ℓ_i the length of the i-th bar, and the compliance $c(\mathbf{x})$ is given by

$$c(\mathbf{x}) = \begin{cases} \mathbf{f}^\top \mathbf{u} & \text{If there exists } \mathbf{u} \text{ such that } \mathbf{K}(\mathbf{x})\mathbf{u} = \mathbf{f}\,, \\ +\infty & \text{otherwise,} \end{cases}$$

where $\mathbf{K}(\mathbf{x})$ denotes the stiffness matrix corresponding to the design $\mathbf{x}$. It is known that $c\colon \mathbb{R}^m \to \mathbb{R} \cup \{+\infty\}$ is a proper lower semi-continuous convex function, and hence measurable when considering the Borel σ-algebra of $\mathbb{R}^n$, see Alvarez and Carrasco (2005) for details. We note that other mechanical constraints, such as global and local buckling, natural frequency constraints, etc., should be considered to obtain practical solutions. However, these can be considered in a later stage of the design process after a suitable topology has been found.

It is well known that optimal structures obtained by this model are unstable from the mechanical point of view, and great effort has been made in order to obtain formulations having robust optimal trusses, see e.g. Achtziger et al. (1992), Ben-Tal and Nemirovski (1997), Alvarez and Carrasco (2005). More precisely, the optimal truss is not able to support the external loading when it is affected by a small perturbation, or it can support it but presenting a high compliance. In the approach named *robust topology optimization of trusses*, the idea is to take into account in some way these small perturbations in order to obtain an optimization model, such that the optimal solution be less sensitive to them. For example, there are deterministic models that consider the worst-case of compliances (Ben-Tal and Nemirovski 1997) or other performance measures (Canelas et al. 2017), when external loads belong to an ellipsoid. The stochastic modeling of the perturbations is also a frequent approach (see Alvarez and Carrasco (2005) where the expected compliance is minimized in the case of stochastic loading). In the same line, Guest and Igusa (2008) studied the case in which uncertainties are considered in loads and also in nodal positions.

RBDO can be used as an alternative approach to obtain a robust design. Despite RBDO leads to more intensive computational models, it has the advantage of considering quantitatively an important measure of performance in engineering applications: the failure probability. The RBDO version of Problem (P_D) replaces the design variable $\mathbf{x}$ and some other problem data by random variables. For instance, consider that $\mathbf{x}$, and $\mathbf{f}$ are replaced by $\tilde{\mathbf{x}}$ and $\tilde{\mathbf{f}}$, which are random variables given by $\tilde{\mathbf{x}} = \mathbf{x} + \mathbf{A}\boldsymbol{\xi}_{\mathbf{x}}$, and $\tilde{\mathbf{f}} = \mathbf{f} + \mathbf{B}\boldsymbol{\xi}_{\mathbf{f}}$, where $\boldsymbol{\xi} = (\boldsymbol{\xi}_{\mathbf{x}}, \boldsymbol{\xi}_{\mathbf{f}})$ is a multivariate normal random variable of zero mean and identity covariance matrix and $\mathbf{A}, \mathbf{B}$ are given matrices. Then, the RBDO version of Problem (P_D) is defined in terms of the design variable $\mathbf{x}$ by

$$\begin{aligned} &\min_{\mathbf{x}} \sum_{i=1}^{m} \ell_i x_i \,, \\ &\text{s.t. } \mathbb{P}\{\Omega(\mathbf{x})\} \geq 1 - P_f \,, \qquad (P_S) \\ &\mathbf{x} \geq 0, \end{aligned}$$

where

$$\Omega(\mathbf{x}) = \{\boldsymbol{\xi} \in \mathbb{R}^m \ : \ c(\mathbf{x}, \boldsymbol{\xi}) \leq c_0 \text{ and } \mathbf{x} + \mathbf{A}\boldsymbol{\xi}_{\mathbf{x}} \geq 0\}, \quad (10)$$

and

$$c(\mathbf{x}, \boldsymbol{\xi}) = \begin{cases} (\mathbf{f}+\mathbf{B}\boldsymbol{\xi}_{\mathbf{f}})^{\top}\mathbf{u} & \text{If there exists } \mathbf{u} \text{ such that } \mathbf{K}(\mathbf{x}+\mathbf{A}\boldsymbol{\xi}_{\mathbf{x}})\mathbf{u} = \mathbf{f}+\mathbf{B}\boldsymbol{\xi}_{\mathbf{f}}, \\ +\infty & \text{otherwise.} \end{cases}$$

In simple words, Problem (P_S) attempts to minimize the expected volume of the truss structure keeping the failure probability below the value P_f. As pointed out by Liu et al. (2016a), Problem (P_S) can be reformulated as a convex one. In fact, since the compliance is a convex function of the bar cross-section areas and the loading (Alvarez and Carrasco 2005), then $c(\mathbf{x}, \boldsymbol{\xi})$ is convex on the variable $(\mathbf{x}, \boldsymbol{\xi})$. This property and the logconcavity property of the multivariate normal probability density function $f_{\boldsymbol{\xi}}$ imply that $\mathbb{P}\{\Omega(\mathbf{x})\}$ be logconcave; see (Prékopa 1995, Theorem 10.2.1). Therefore, a convex problem is obtained if the probability constraint is reformulated as $\log(1 - P_f) - \log\left(\mathbb{P}\{\Omega(\mathbf{x})\}\right) \leq 0$.

Unfortunately, in the approximate version of (P_S) obtained following the proposed method, the probability constraint loses the convexity property. This is due to the fact that the domain $\tilde{\Omega}(\boldsymbol{\xi}_1(\mathbf{s}), \ldots, \boldsymbol{\xi}_k(\mathbf{s}))$ of Fig. 1 can be nonconvex, so that it cannot be described by a set of convex constraints even in the case that a convex safe region is found at the solution. The following approximate version of (P_S) is considered here:

$$\begin{aligned} &\min_{\mathbf{x},\mathbf{s}} f(\mathbf{x}), \\ &\text{s.t. } c(\mathbf{x}, \boldsymbol{\xi}_i(\mathbf{s})) \leq c_0, \quad \text{for } i = 1, \ldots, k, \qquad (P_{SA}) \\ &P_f(\mathbf{s}) \leq P_f, \\ &\mathbf{x} \geq \varepsilon. \end{aligned}$$

Only the loadings are modeled as random variables. The small value $\varepsilon > 0$ is considered to obtain a smooth compliance, which is necessary since no special reformulation of the problem will be used. The constraint function $P_f(\mathbf{s})$ provides the failure probability as detailed in Section 3. To represent the approximate limit state surface, we consider a mesh of $d \times \cdots \times d \times 2d$ intervals for Θ, with $d = 4$ or $d = 8$. To compute the failure probability each of the $d \times d \times \cdots \times d \times 2d$ hyper-cubes of the mesh was divided into $3 \times 3 \times \cdots \times 3$ elements, and the integration of the failure probability in the elements was obtained by Gaussian quadrature with only one integration point. The examples are solved by using the interior-point algorithm *fmincon* of MATLAB, which has the possibility of using second order sensitivity information. Although the Hessian matrix of the problem is full and difficult to compute, it was noticed that it provides for a significant reduction of the time spent by *fmincon* thanks to a considerable reduction of the number of iterations required to satisfy the stopping criteria. In fact, by using the profile tools of MATLAB, we notice that most of the time of solution is spent in the factorization of the internal linear systems of *fmincon*; the computation of the performance functions (including the failure probability) and their first and second derivatives is a relatively inexpensive task. In all the examples, the default tolerance values for the stopping criteria of *fmincon* were considered. The value $\varepsilon = 0.001\,\text{m}^2$ was used as a lower bound of the cross-sectional area. The examples were solved in a PC with an Intel core i7-6700 CPU. To improve the visibility of the optimized solutions, only the bars with a cross-sectional area higher than 1 % of the largest cross-sectional area of the solution are drawn in the pictures.

Example 1 (*Crane arm*) The geometry, loadings and failure probability of this example are taken from Liu et al. (2016a) (see Fig. 11). The target failure probability of this example corresponds to a reliability index $\beta = 2$. Two different

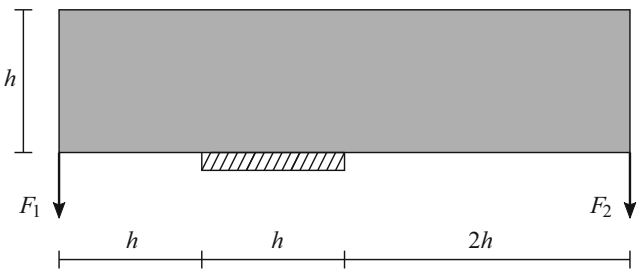

Fig. 11 Example 1: Crane arm. The bars join the nodes on a grid inside the rectangle of height $h = 1$ m, and are composed by a linear elastic material with Young's modulus $E = 100$ Pa. The forces F_1 and F_2 are of 1 N of magnitude. The random loading is $7F_1 + 3\xi_1 F_1 + 7F_2 + 3\xi_2 F_2$ with (ξ_1, ξ_2) a multivariate normal random variable with zero mean and identity covariance matrix

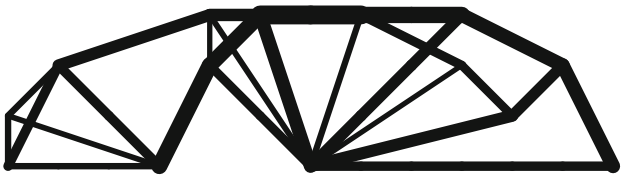

Fig. 12 Example 1a: Crane arm. Result obtained for the mesh of 13×4 nodes, $d = 8$

meshes are considered: the case a) with 13×4 nodes with level 6 nodal connectivity, see Liu et al. (2016a), which corresponds to 629 non-overlapping bars; and the case b) with 17×5 nodes and full connectivity, corresponding to 2196 non-overlapping bars. The solutions obtained are shown by Figs. 12 and 13.

Example 2 (*Short bridge*) The geometry and loadings of this example are taken from Makrodimopoulos et al. (2009). We reduced the height in reason of the solutions presented in that paper (see Fig. 14). The target failure probability of this example corresponds to a reliability index $\beta = 3$. Two different meshes are considered: the case a) with 13×7 nodes, which corresponds to 2542 non-overlapping bars; and the case b) with 17×9 nodes, corresponding to 7180 non-overlapping bars. The solutions obtained are shown by Figs. 15 and 16.

Example 3 (*3D Beam*) In this case, the clamped beam of Fig. 17 is considered. The beam is submitted to bending in vertical and horizontal directions, and also torsion. The target failure probability of this example corresponds to a reliability index $\beta = 3$. A mesh of $3 \times 3 \times 9$ nodes and full connectivity, which corresponds to 2660 non-overlapping bars is considered. The solution obtained is shown by Fig. 18.

Table 2 presents the results obtained. All the examples were solved successfully, i.e., the optimization algorithm was able to find designs with the optimality measures required by the stopping criteria. The number of iterations

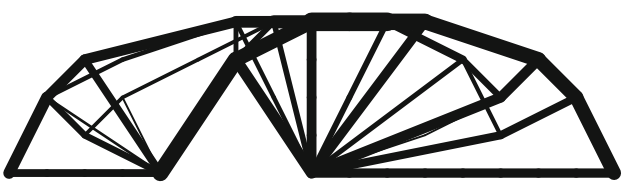

Fig. 13 Example 1b: Crane arm. Result obtained for the mesh of 17×5 nodes, $d = 8$

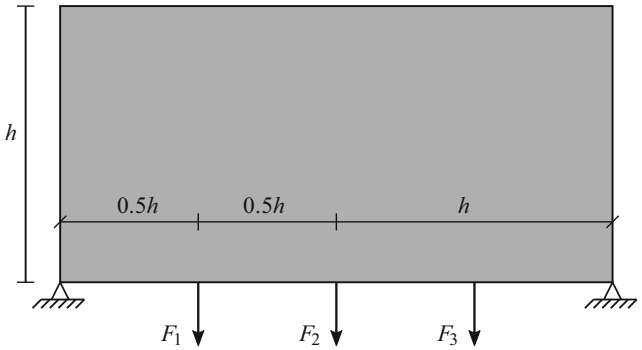

Fig. 14 Example 2: Short bridge. The bars join the nodes on a grid inside the rectangle of height $h = 0.5$ m, and are composed by a linear elastic material with Young's modulus $E = 1$ Pa. The forces F_1–F_3 are of 1 N of magnitude. The random loading is $\xi_1 F_1 + \xi_2 F_2 + \xi_3 F_3$ with (ξ_1, ξ_2, ξ_3) a multivariate normal random variable with zero mean and identity covariance matrix

was similar in all the examples, with a maximum of 41. Despite the fact that the optimization model is not convex, convergence difficulties were not observed when considering the examples presented or other similar ones. The table shows the reliability index β of the optimized structures, which were computed by using the same techniques of Section 3, considering a fine mesh for the exact limit state surface. The table shows that a mesh of $d \times \cdots \times d \times 2d$ intervals with $d = 4$ provides structures with a reasonable reliability index. When using $d = 8$ excellent results were obtained, with a deviation of less than 2 % in the target reliability index. Note that the optimized structures of Example 2b) are slightly heavier than the corresponding ones of Example 2a). The reason of that strange fact is that the minimum cross-sectional area ε implies that certain volume of material cannot be redistributed. This volume is of only 1.05 m^3 in Example 2a), but it rises to 3.06 m^3 in Example 2b).

4.1 Comparison with FORM

In this section, we present a comparison of the proposed technique with FORM, one of the most popular methods

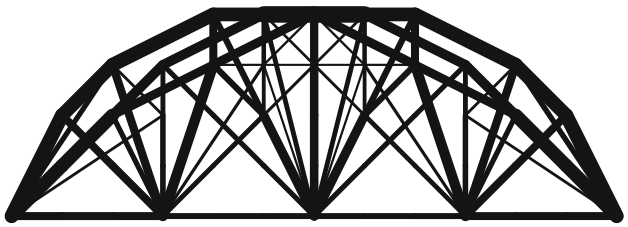

Fig. 15 Example 2a: Short bridge. Result obtained for the mesh of 13×7 nodes, $d = 8$

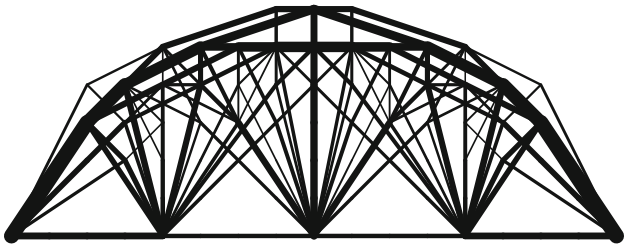

Fig. 16 Example 2b: Short bridge. Result obtained for the mesh of 17×9 nodes, $d = 8$

used in reliability analysis. We use FORM to define the following approximate version of (P_S):

$$\begin{aligned} &\min_{\mathbf{x}} \sum_{i=1}^{m} \ell_i x_i, \\ &\text{s.t. } \mathbb{P}\{\hat{\Omega}(\boldsymbol{\xi}^*(\mathbf{x}))\} \geq 1 - P_f, \qquad (P_F) \\ &\mathbf{x} \geq \varepsilon, \end{aligned}$$

where $\hat{\Omega}(\boldsymbol{\xi}^*(\mathbf{x}))$ is the half space $\{\boldsymbol{\xi} : (\boldsymbol{\xi}^*(\mathbf{x}) - \boldsymbol{\xi}) \cdot \boldsymbol{\xi}^*(\mathbf{x}) \geq 0\}$ and $\boldsymbol{\xi}^*(\mathbf{x})$ is the MPP defined as the point in the original failure surface with maximum probability density. For a multivariate normal random variable with zero mean and identity covariance matrix, $\boldsymbol{\xi}^*(\mathbf{x})$ is the point in the original failure surface with minimum norm. The small value $\varepsilon > 0$ has the same role as in (P_{SA}).

Let us consider the topology optimization problem with a random load $\mathbf{f} = F_1\xi_1 + \ldots + F_k\xi_k$, i.e., $\mathbf{f} = \mathbf{F}\boldsymbol{\xi}$ where the matrix $\mathbf{F}$ has columns F_i. In this problem, there is a closed formula for the MPP: $\boldsymbol{\xi}^*(\mathbf{x}) = (c_0/\mu(\mathbf{x}))^{1/2}\mathbf{v}(\mathbf{x})$, where c_0 is the lower bound on the compliance, $\mu(\mathbf{x})$ is the maximum eigenvalue of $\mathbf{M}(\mathbf{x}) = \mathbf{F}^\top \mathbf{K}(\mathbf{x})^{-1}\mathbf{F}$, and $\mathbf{v}(\mathbf{x})$ is the unit eigenvector associated to $\mu(\mathbf{x})$, see Appendix. The closed formula shows that the MPP is never unique: $\boldsymbol{\xi}^*(\mathbf{x})$ and $-\boldsymbol{\xi}^*(\mathbf{x})$ are both MPPs. In addition, if the maximum eigenvalue $\mu(\mathbf{x})$ is multiple, then the MPP will not be unique

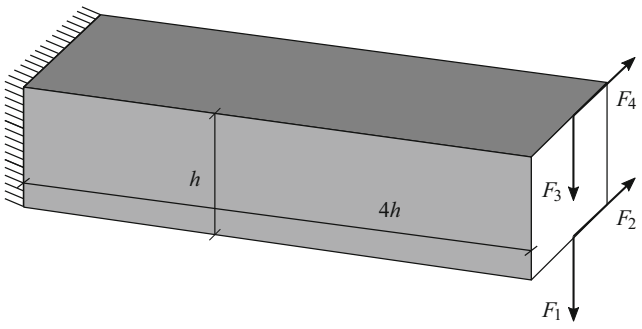

Fig. 17 Example 3: 3D beam. The bars join the nodes on a grid inside the prism which has a square cross-section of height $h = 1$ m, and are composed by a linear elastic material with Young's modulus $E = 100$ Pa. The forces F_1–F_4 are of 1 N of magnitude. The random loading is $\xi_1 F_1 + 0.3\xi_2 F_2 + \xi_3 F_3 + 0.3\xi_4 F_4$, with $(\xi_1, \xi_2, \xi_3, \xi_4)$ a multivariate normal random variable of zero mean and identity covariance matrix

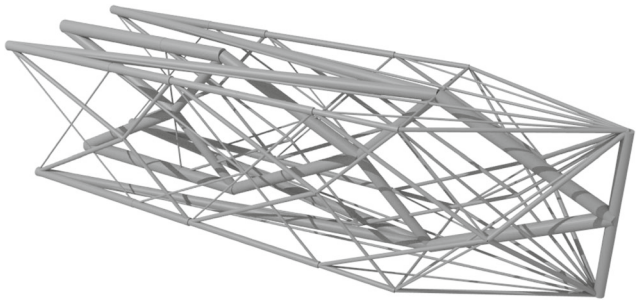

Fig. 18 Example 3: 3D beam. Result obtained for $d = 8$

even locally, a fact that may affect the order of convergence of the optimization algorithms used to find the MPP. In addition, the closed formula shows that the MPP could not depend continuously on the project variable $\mathbf{x}$, since we may have an abrupt jump of the eigenvector at a point where the two maximal eigenvalues equal each other. In this particular problem, we may use the closed formula instead of the usual optimization approach to find the MPP, with the advantage that the closed formula is fast, accurate and highly reliable for low-dimensional random spaces.

In view of the two possibilities for finding the MPP, we will consider the *short bridge* and the *3D beam* examples of Figs. 14 and 17 (in both examples the random force is $\mathbf{f} = \mathbf{F}\boldsymbol{\xi}$), and solve several instances of them. In the case of the short bridge four meshes are considered: a) 5×3, b) 9×5, c) 13×7 and d) 17×9 nodes. Four cases are also considered for the 3D beam: a) $3 \times 3 \times 3$, b) $3 \times 3 \times 5$, c) $3 \times 3 \times 7$ and d) $3 \times 3 \times 9$ nodes. Full connectivity is considered in all cases. The three methods used to solve the examples are the following:

Proposed method As described in the previous section, it consists of solving (P_{SA}) for a Polytope approximation with $d = 8$. The problem was solved using the interior-point algorithm *fmincon* of MATLAB provided with second order sensitivity information. The default tolerance values for the stopping criteria of *fmincon* were considered.

FORM1 It consists of solving (P_F) using the interior-point algorithm *fmincon* of MATLAB provided with first order sensitivity information (this is the usual approach when using FORM). The MPP is found by using the closed formula. The default tolerance values for the stopping criteria of *fmincon* were considered, except for the variable *StepTolerance* which was set equal to 10^{-4} (the default value is 10^{-6}) to avoid the large number of iterations, without significant improvement of the solution that was observed when using the default value.

FORM2 The same of FORM1, but in this case, the MPP is found by using *fmincon* instead of the closed formula, i.e.

Table 2 Results obtained

Example	elem	d	var	con	vol (m^3)	β	iter	time (s)
Crane arm a)	629	4	638	10	295.63	2.039	33	6.1
Crane arm a)	629	8	646	18	291.32	2.008	28	4.9
Crane arm b)	2196	4	2205	10	290.58	2.042	32	131.1
Crane arm b)	2196	8	2213	18	286.01	2.009	32	135.5
Short bridge a)	2542	4	2587	46	53.59	3.244	37	193.1
Short bridge a)	2542	8	2695	154	48.36	3.054	36	194.8
Short bridge b)	7180	4	7225	46	53.97	3.245	41	4132.2
Short bridge b)	7180	8	7333	154	48.80	3.055	40	4369.1
3D beam	2660	4	2885	226	158.82	3.431	40	301.5
3D beam	2660	8	4037	1378	128.26	3.032	32	743.9

Notations: *elem*: number of potential elements, d: value used in the mesh of $d \times \cdots \times d \times 2d$ intervals for Θ, *var*: number of optimization variables, *con*: number of constraints, *vol*: volume of the optimized structure, β: reliability index of the optimized structure, *iter*: number of iterations, *time*: time spent in the solution

in this case we have a nested iteration. The optimization problem of the inner iteration involves a quadratic objective with a quadratic constraint (see Appendix), and second order sensitivity information was used to reduce the number of iterations. The variable *StepTolerance* was set equal to 10^{-7} in the inner iteration to improve the accuracy in the determination of the MPP. For the outer iteration, we used the same tolerance values used in FORM1.

Note that FORM1 and FORM2 are used to solve the same problem (P_F). The only difference in these approaches is the procedure used to find the MPP. Then, if both algorithms are successful, they should find the same solution. The proposed approach is based on a fairly different approximation of the safe region, which can lead to a substantially different solution as we will show below.

Tables 3 and 4 present the results obtained. Table 3 shows that FORM1 and FORM2 tend to obtain lighter structures. However, the reliability indices of the optimized structures are much lower than the target $\beta = 3$ of these examples. The proposed approach with $d = 8$ instead provides structures with a reliability index quite close to the target one. As noted in previous sections, the proposed approach tends to overestimate the failure probability, which leads to a final reliability index slightly higher than the target one. Table 4 shows the number of iterations and the time required by the three approaches to find the solution. FORM2 generally required fewer iterations and less time than FORM1. However, in some examples solved with FORM2 the algorithm *fmincon* reported that it was not able to reach the default tolerance in the constraint violation (examples indicated by the highlighted figures in the table). FORM1 was in all cases able to find a solution satisfying the default tolerances, which shows that the convergence difficulties experienced by FORM2 were probably due to an inaccurate determination of the MPP. The proposed approach solved all the examples satisfying the default tolerances of *fmincon*,

Table 3 Results obtained with the proposed method, FORM1, and FORM2: volume and reliability index

Example	elem	vol (m^3)			β		
Short bridge a)	74	56.23,	40.18,	40.42	3.048,	2.161,	2.152
Short bridge b)	632	49.25,	35.94,	*43.54*	3.046,	2.125,	*2.125*
Short bridge c)	2542	48.36,	41.75,	*41.82*	3.054,	2.124,	*2.119*
Short bridge d)	7180	48.80,	38.88,	*39.35*	3.055,	2.115,	*2.117*
3D beam a)	302	153.5,	122.9,	*122.7*	3.032,	2.029,	*2.078*
3D beam b)	832	131.5,	108.1,	108.1	3.032,	2.178,	2.174
3D beam c)	1618	129.2,	109.1,	109.1	3.032,	2.100,	2.149
3D beam d)	2660	128.3,	104.9,	104.9	3.032,	2.173,	2.167

Notations: *elem*: number of potential elements, *vol*: volume of the optimized structure, β: reliability index of the optimized structure. The highlighted figures indicate the results where *fmincon* reported convergence difficulties

Table 4 Results obtained with the proposed method, FORM1, and FORM2

Example	elem		iter		time (s)		
Short bridge a)	74	36,	84,	42	2.2,	1.2,	10.9
Short bridge b)	632	34,	81,	*56*	8.5,	16.4,	*16.4*
Short bridge c)	2542	36,	108,	*45*	194.8,	1580.9,	*88.0*
Short bridge d)	7180	40,	189,	*71*	4132.2,	41771.9,	*2432.9*
3D beam a)	302	25,	144,	*56*	17.6,	10.0,	*10.0*
3D beam b)	832	28,	123,	124	105.0,	24.4,	32.0
3D beam c)	1618	29,	208,	216	263.1,	335.6,	244.5
3D beam d)	2660	32,	209,	153	743.9,	1989.5,	508.2

Notations: *elem*: number of potential elements, *iter*: number of iterations, *time*: time spent in the solution. The highlighted figures indicate the results where *fmincon* reported convergence difficulties

requiring calculation times comparable to those required by FORM2.

In conclusion, the proposed approach leads to optimized structures with a reliability index quite close to the target one in a reasonable calculation time. Therefore, it can be considered as an adequate alternative to FORM for the solution of this type of topology optimization problems. Two features of the proposed approach can be seen as additional advantages: it tends to provide structures with a reliability index higher than the target one (the solution obtained is therefore feasible with respect to the original probability constraint), and it does not require the determination of the MPP, i.e., situations with multiple MPPs will not be particularly difficult.

5 Conclusions

In this paper, we have introduced a new method for reliability analysis and reliability-based design optimization, which is based on a polytope-like description of the safe region. The shape of the polytope depends on the position of a set of control points which in their turn depend on a set of shape variables. In the space of the angular variables of the generalized spherical coordinates, the polytope is defined by a regular mesh, which is used to compute approximately the failure probability and its sensitivities with respect to the shape variables.

The method is appropriate for problems where the safe region is star-shaped with respect to the origin. An accurate representation of the failure surface requires a number of control points that increases exponentially with the dimension of the random space. Therefore, the method proposed is appropriate only for low-dimensional random spaces. If this is the case, then the method proposed can be used instead of the first and second order reliability ones, when they fail to provide the failure probability with sufficient accuracy.

We have presented an application of the method proposed to the topology optimization problem of truss structures. For this problem, the method allows the computation of the second derivatives of the probability constraint. Several medium-scale optimization examples were successfully solved.

Acknowledgements Alfredo Canelas thanks the Uruguayan Councils ANII and CSIC for the financial support.

Funding information This research was supported by CONICYT-Chile, via FONDECYT project 1160894.

Appendix: Closed formula for the MPP

Since the random load is $\mathbf{f} = \mathbf{F}\boldsymbol{\xi}$, and $\mathbf{x} \geq \varepsilon$, then $c(\mathbf{x}, \boldsymbol{\xi}) = \boldsymbol{\xi}^\top \mathbf{F}^\top \mathbf{K}(\mathbf{x})^{-1} \mathbf{F}\boldsymbol{\xi}$. By calling $\mathbf{M}(\mathbf{x}) = \mathbf{F}^\top \mathbf{K}(\mathbf{x})^{-1}\mathbf{F}$, we have that the MPP can be found as the solution $\boldsymbol{\xi}^*$ to

$$\min_{\boldsymbol{\xi}} \boldsymbol{\xi}^\top \boldsymbol{\xi} \,,$$
$$\text{s.t. } \boldsymbol{\xi}^\top \mathbf{M}(\mathbf{x}) \boldsymbol{\xi} \geq c_0 \,.$$

Note that the inequality constraint must be active at the solution (the MPP is in the failure surface), since the only possible interior solution is $\boldsymbol{\xi}^* = 0$ which does not satisfy the constraint for a positive c_0. Hence, let λ be the nonnegative Lagrange multiplier of the constraint at the solution. The first order optimality condition is $\boldsymbol{\xi}^* - \lambda \mathbf{M}(\mathbf{x})\boldsymbol{\xi}^* = 0$. The value $\lambda = 0$ is not a possible solution since it leads to $\boldsymbol{\xi}^* = 0$. Hence $\lambda > 0$. Let $\mu = \lambda^{-1}$. Then, from the optimality condition we obtain $\mathbf{M}(\mathbf{x})\boldsymbol{\xi}^* = \mu\boldsymbol{\xi}^*$. Hence $\boldsymbol{\xi}^*$ must be an eigenvector of $\mathbf{M}(\mathbf{x})$ of eigenvalue μ. Let $\mathbf{v}$ be a unit eigenvector of eigenvalue μ, i.e. $\mathbf{M}(\mathbf{x})\mathbf{v} = \mu\mathbf{v}$ with $\mathbf{v}^\top\mathbf{v} = 1$. Then $\boldsymbol{\xi}^* = \alpha\mathbf{v}$ for certain value α. Since the constraint is active $\boldsymbol{\xi}^{*\top}\mathbf{M}(\mathbf{x})\boldsymbol{\xi}^* = \alpha^2\mathbf{v}^\top\mathbf{M}(\mathbf{x})\mathbf{v} = \alpha^2\mu = c_0$. Then $\alpha^2 = c_0/\mu$ and $\boldsymbol{\xi}^* = \alpha\mathbf{v} = (c_0/\mu)^{1/2}\mathbf{v}$. Since the objective function is $\boldsymbol{\xi}^{*\top}\boldsymbol{\xi}^* = \alpha^2 = c_0/\mu$, then μ must be the maximum eigenvalue of $\mathbf{M}(\mathbf{x})$.

References

Achtziger W (1997) Topology optimization of discrete structures: an introduction in view of computational and nonsmooth aspects. In: Topology optimization in structural mechanics, CISM courses and lectures, vol 374. Springer, Vienna, pp 57–100

Achtziger W, Bendsøe M, Ben-Tal A, Zowe J (1992) Equivalent displacement based formulations for maximum strength truss topology design. Impact of Computing in Science and Engineering 4(4):315–345

Alvarez F, Carrasco M (2005) Minimization of the expected compliance as an alternative approach to multiload truss optimization. Struct Multidiscip Optim 29(6):470–476

Ben-Tal A, Nemirovski A (1997) Robust truss topology design via semidefinite programming. SIAM J Optim 7(4):991–1016

Bendsøe M (1995) Optimization of structural topology, shape and material. Springer, Berlin

Canelas A, Carrasco M, López J (2017) Application of the sequential parametric convex approximation method to the design of robust trusses. J Glob Optim 68(1):169–187

Choi SK, Grandhi RV, Canfield RA (2007) Reliability-based structural design, 1st edn. Springer, London

Ditlevsen O, Madsen HO (1996) Structural reliability methods, 1st edn. Wiley, Chichester

Dorn WS, Gomory RE, Greenberg HJ (1964) Automatic design of optimal structures. Journal de Mecanique 3:25–52

Guest J, Igusa T (2008) Structural optimization under uncertain loads and nodal locations. Comput Methods Appl Mech Eng 198(1):116–124

Herskovits J, Mappa P, Goulart E, Mota Soares CM (2005) Mathematical programming models and algorithms for engineering design optimization. Comput Methods Appl Mech Eng 194(30–33):3244–3268

Liu K, Paulino GH, Gardoni P (2016a) Reliability-based topology optimization using a new method for sensitivity approximation—application to ground structures. Struct Multidiscip Optim 54(3):553–571

Liu K, Paulino GH, Gardoni P (2016b) Segmental multi-point linearization for parameter sensitivity approximation in reliability analysis. Struct Saf 62:101–115

Makrodimopoulos A, Bhaskar A, Keane AJ (2009) Second-order cone programming formulations for a class of problems in structural optimization. Struct Multidiscip Optim 40(1):365–380. https://doi.org/10.1007/s00158-009-0376-2

Prékopa A (1995) Stochastic programming, mathematics and its applications, vol 324. Kluwer Academic Publishers Group, Dordrecht. https://doi.org/10.1007/978-94-017-3087-7

Rackwitz R (2001) Reliability analysis—a review and some perspectives. Struct Saf 23(4):365–395

Schuëller GI, Jensen HA (2008) Computational methods in optimization considering uncertainties – an overview. Comput Methods Appl Mech Engrg 198(1):2–13

Tu J, Choi KK, Park YH (2001) Design potential method for robust system parameter design. AIAA J 39:667–677

Uryas'ev S (1994) Derivatives of probability functions and integrals over sets given by inequalities. J Comput Appl Math 56:197–223